

Improvement of Cryogenic Space Rocket Engine Ignition: inert gas sweep effects

Philippe Fauquet-Alekhine^{1*}

¹Lab. for Research in Science of Energy, Montagret, France

ABSTRACT

Ignition of cryogenic engines of space launchers is usually preceded by a transient phase during which feeding lines of the combustion chamber are swept by an inert gas. This sweeping flow may be prolonged for several milliseconds while propellants injection begins.

Despite the fact that this transient may generate instabilities influencing the ignition process, related oscillations have not been investigated. Experiments were carried out with nitrogen flowing in a full scale injector of HMB7 engine (equipping Ariane 5 launcher) in thermo-hydrodynamic conditions of similitude with oxygen flow in HM7B (actual oxidizer propellant of HM7B). Two conditions were investigated: 1) with nitrogen only, 2) with helium gas injected simultaneously with nitrogen during the initial 150 milliseconds. The aim was to characterize the instabilities occurring during a pre-ignition transient of 300ms and the effect of the inert gas sweep on these instabilities.

Impact force of the jet, density and pressure at injector exit were measured by means of load cell, piezoresistive sensor and resonance cavity respectively. Mass flow was then calculated through momentum equation and slip ratio correlation.

Measurements and analysis showed that the flow was inverted annular flow and mist flow, instabilities were of thermoacoustic oscillation (TAO) type, and led to suggest the thermal effect as the major effect in the production of these oscillations. This also showed that a prolonged sweep of the injector with inert gas had a stabilizing effect on the two-phase flow due to the reduction of wall heat flux and of the inlet subcooling enthalpy. This finding is of great interest also because it shows that TAO are generated in the unit engine much earlier than ignition inside the combustion chamber. Possible coupling between these TAO and those occurring after ignition during combustion (which have different source and with different sustaining factors) might bring interesting knowledge regarding engine ignition process.

Keywords: Space rocket; Cryogenic engine; Ignition; Two-phase; Nitrogen; Instabilities; Oscillations

1. INTRODUCTION

Ignition of cryogenic space rocket engines are key phases for space flights. Without appropriate ignition (especially in terms of time and power delivered), the space mission may be compromised. In recent years, with the proliferation of projects aiming at developing engines with re-ignition [1-5], new stakes have been raised regarding ignition, the expected benefit being to ship multiple payloads, to place satellites closer to their final orbits. The control of ignition or re-ignition phases depending on a pre-ignition transient is a crucial

* Tel.: +33247987804; fax: +33247987809.
E-mail address: larsen.sciences@yahoo.fr

challenge: an ignition failure or a long lasting ignition may lead to lose control of the launcher or to make the engine exploding after gases accumulation inside the combustion chamber, thus destroying payloads [6].

Cryogenic space rocket engines may operate at low or high pressure in nominal conditions depending on the technology used but anyway ignition comes through a pre-ignition transient, a phase of low pressure before launching turbopumps necessary to reach high pressure [7].

Propulsion units including cryogenic engine respect a similar design [6, 8] (Figure 1): mainly a combustion chamber in which the propellants are injected through coaxial injectors, a nozzle whereby the combustion gases reach the required speeds necessary for propulsion purpose, two propellant supply turbopumps themselves operated by a portion of the resulting combustion gases, two tanks of hydrogen and oxygen (LH2 and LOX) under low pressure (example Figure 2). Propellants are injected at cryogenic temperature. Oxygen enters a cavity called LOXdome and is supplied to combustion chamber through several tens or hundreds of injectors located under the bottom plate of the dome (predistributor plate). Hydrogen enters a toroidal collector and is distributed in a bundle of rectangular channels within the combustion chamber wall. It then flows up to the predistributor plate and the H2 flow surrounds the LOX flow through coaxial injectors [9-12].

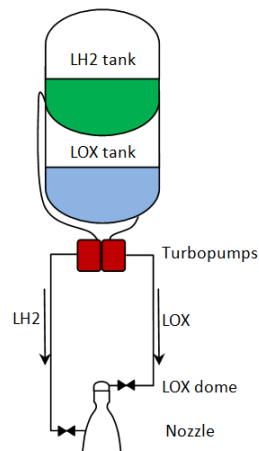


Fig. 1. Schematic design of a cryogenic unit (type HM7B of Ariane launcher)

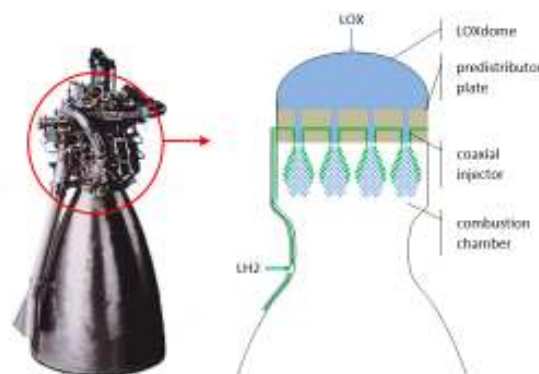


Fig. 2. HM7B engine and the schematic design of its combustion chamber (Source:

The pre-ignition transient always goes through a sequence in four steps: sweep of propellant ducts with inert gas for complete purge, H₂ fill without combustion, start-up of the igniter, admission of the oxidizer O₂. The time lasting between H₂ admission and ignition generally lasts several hundreds of milliseconds [13]. The time between admission of O₂ and ignition lasts generally a few hundreds of milliseconds. This procedure creates an insufficient mixture before ignition because an oxidant mixture would destroy the engine walls [14:p30]. This transient combines different types of oscillations due to the temperature difference between the cryogenic propellants and the walls in the LOX dome [15]. Even with a pre-cooling of the feeding system, this difference is high enough to produce oscillations. This complex thermo-hydraulic instabilities do not facilitate ignition [16] whereas short time ignition is expected and favored by stable and homogeneous mixture described by specialists as propellants "intimately and uniformly mixed" [17:p92].

The aim of the present study is to characterize the possible benefits of inert gas sweep management in order to reduce oscillations during the pre-ignition transient of cryogenic engines and thus to favor a quick ignition.

2. MATERIAL AND METHODS

2.1. Design

Experiments were carried out on a mock-up representing LOX supply simulated by liquid nitrogen (LN₂) in one injector during a pre-ignition transient of 300 ms (time after which effectiveness of ignition is expected). LN₂ was stored in a pressurized and insulated tank. LN₂ was led to the injector through a duct closed by a solenoid gate valve (LN₂ valve) to be opened in less than 5ms in cryogenic conditions: this was verified by high speed camera. Downstream this valve, a cavity reproduced the LOX dome connected to the injector reproducing one HM7B injector full-scale. Material used to build the mock-up was stainless steel as done for HM7B engine. Dimensions and material being similar to real operating conditions, calculations of similitude for the flow was only based on Reynolds number and data given for the cryogenic engine HM7B [13, 18]: LN₂ was thus stored at constant pressure and temperature conditions equal to 3.5bar and 77K representing pre-ignition conditions before launching turbopumps. Inert gas sweep was made possible, done as for the rocket engine with helium gas (He) injected into the LOX dome; with similitude to HM7B, the flow rate was .1g/s for one injector [13] maintained constant and independent from downstream pressure by creating a sonic flow through a micrometric valve. Two experimental conditions were studied: 1) with inert gas sweep before opening the LN₂ valve only, 2) with inert gas sweep before opening the LN₂ valve and 150ms after.

The injector was made up of five parts: a converging part (angle: 15°, length: 1.5mm), inlet (diameter: 2mm, length: 3 mm), diverging part (angle: 51°, length: 1mm), cylindrical part (diameter: 4.5mm, length: 14.5mm), converging part (angle: 37°, length: 1mm), outlet part (diameter: 3mm, length: 18mm). Along the injector, pressure was measured in three points by piezoresistive sensors: before inlet (according to the fluid flow) p_1 , entrance constriction p_2 , before exit p_3 . At the exit of the injector where external pressure p_4 , void fraction and thrust were measured by means resp. of a microwave resonator and a plate mounted on a piezoelectric load cell (Figure 3). This metrology is described in section 2.2. Measurements of these parameters acquired at 5ms interval allowed us to calculate the mass flow rate G vs pressure drop $dp=p_3-p_4$ at the exit as described in section 2.3.

102
 103 Characterization of N2 flow for each experimental condition was considered in terms of G
 104 and dp and instability types.



105
 106 **Fig. 3. LN2 two-phase jet exiting the injector (vertical flow) and impacting the plate**
 107 **mounted on load cell: the N2 flow goes upwards on the picture**

108 From the expression of the volume balance in dotted line on Figure 4 applying momentum
 109 conservation equation, we derived the total N2 mass flow G at injector exit:
 110

$$111 \quad Gv = F - A_{exit} (p_3 - p_4) \quad (1)$$

112 with:

$$113 \quad G = F - A_{exit} \sum_{i=l,g} \alpha_i \rho_i v_i \quad (2)$$

114 Introducing the slip factor $s = v_g/v_l$, (2) becomes:

$$115 \quad G = F - A_{exit} [s \alpha_g \rho_g + \alpha_l \rho_l] v_l \quad (3)$$

116 Introducing:

$$117 \quad f = F - A_{exit} (p_3 - p_4) \quad (4)$$

$$118 \quad \rho_m = \alpha \rho_g + (1 - \alpha) \rho_l \quad (5)$$

$$119 \quad X = G_g/G \quad (6)$$

120 equation (3) into (1) gives:

$$121 \quad G^2 = A_{exit} \rho_m f \xi(X; s) \quad (7)$$

122 where ξ is a function defined as:

$$123 \quad \xi(X; s) = \{1 + X(1 - X)(s + 1/s - 2)\}^{-1} \quad (8)$$

124 Calculations showed that for the expected values of G and α in the considered experimental
 125 conditions, the function ξ could be approximated by 1 with negligible error on G ;
 126 demonstration follows.
 127

128 Estimating the slip factor s using Premoli et al.'s [19] correlation which has the benefit of
 129 taking into account the mass flow (established for vertical adiabatic flows but tested with
 130 many other types and recommended by the comparative analysis in [20, 21]) defined by:

$$131 \quad s = 1 + E_1 \left(\frac{y}{1+yE_2} - yE_2 \right)^{1/2} \quad (9)$$

132 with:

$$133 \quad y = \frac{\beta}{1-\beta} \quad (10)$$

$$134 \quad \beta = \left(1 + \frac{\rho_g}{\rho_l} \left(\frac{1}{X} - 1 \right) \right)^{-1} \quad (11)$$

$$135 \quad E_1 = 1.578 Re^{-.19} \left(\frac{\rho_l}{\rho_g} \right)^{.22} \quad (12)$$

$$136 \quad E_2 = .0273 We Re^{-.51} \left(\frac{\rho_l}{\rho_g} \right)^{-.08} \quad (13)$$

$$137 \quad Re = \frac{G d_{exit}}{A_{exit} \eta_l} \quad (14)$$

$$138 \quad We = \frac{G^2 d_{exit}}{A_{exit}^2 \gamma \rho_l} \quad (15)$$

139 calculations showed that, for a given value of G , slip ratio increases with quality until a
 140 threshold after which it decreases and tends to 1. At fixed $G=5g/s$, slip ratio is 1 when $X>.7$.
 141 With higher values of G , this threshold is diminishing. In our experiments, G being very early
 142 higher than 5g/s and X being calculated close to 1 led to consider $s=1$ and thus $\xi =1$.
 143 Therefore, for the considered experimental conditions, the error on G using (7) with ξ
 144 approximated by 1 was estimated less than 5.6% according to the comparative study of
 145 Yashar [20] assessing the reliability of correlations for flows in smooth millimetric tubes.

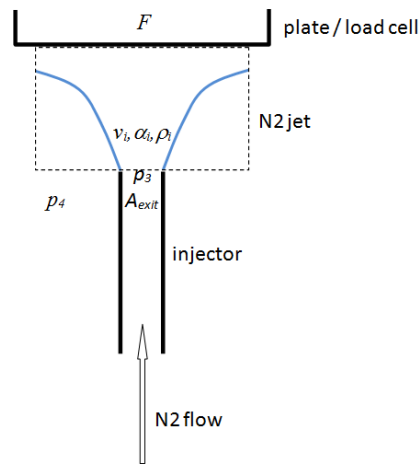


Fig. 4. Sketch of the N2 jet at injector exit impacting plate

148 2.2. Apparatus

2.2.1 Pressure

Along the injector, pressure was measured in three points (nozzle diameter: .4mm) by miniature piezoresistive sensors: sensitivity 5pC/bar, resonance frequency >400kHz, pressure range 0-200bar, rise time 1μm, resolution 0.005bar, linearity <±1%, hysteresis <1%, temperature range -196 to +240°C, temperature coefficient sensitivity $2 \cdot 10^{-4}$ /°C. The response time of these pressure lines was estimated less than 20ms when $(\rho, dp) < (5\text{kg/m}^3; 0.1\text{bar})$ and less than 5ms for higher values which was the case for more than 90% of the acquired signals.

2.2.2 Force

Thrust of the jet at injector exit was measured by means of a plate mounted on a piezoelectric load cell the specifications of which were: sensitivity 46.8pC/N, resonance frequency >400kHz, pressure range -500 to +500N, resolution 0.005N, linearity <±1%, hysteresis <1%, temperature range -115 to +240°C, temperature coefficient sensitivity $2 \cdot 10^{-4}$ /°C.

2.2.3 Density

Density measurement was the most delicate part of the metrology. Two-phase flow density was estimated by means of a cylindrical hyperfrequency resonator (cavity) located at the exit of the injector (Figure 5) inside which the fluid flew along its axis. The method permitted calculation of the fluid density ρ_m from measurement of resonance frequency of the resonator which varies with the dielectric permittivity of the fluid. Its principle was fully described by Krupka [22] or Paez et al. [23]. The method was used since long [see for example 24-28] and applied with many types of resonator [22, 27-28].

The volume considered for measurements was made up of three coaxial media (the fluid flow in the center, the duct wall, the inside of the cavity). In order to optimize measurements, the resonator was designed so that:

- the resonance mode would concentrate the electric energy where the fluid flew giving thus a high sensitivity to variation of the fluid dielectric permittivity and thus to resonance frequency variation,
- a homogenous sensitivity all over the measured volume of fluid was sought implying an optimal homogeneity of the electric field,
- the conditions of resonance would be optimal,
- it avoided overlapping of several resonance modes,
- the cavity was as small as possible (small measurement volume for accuracy and reduced bulk for easier implementation).

As a result, the TM_{010} mode was chosen for the cavity. This mode is quite distinct from others in case of cylindrical resonator (no overlapping) [29]. It presents dominant electric axial component with maximum at the resonator axis while the magnetic field has only azimuthal component. In his review article, Krupka [22] argued this mode creates practical measurement difficulties such as "any air gaps between sample and metal surfaces introduce significant errors in real permittivity determination" (p.62). This drawback, effective for permittivity measurements of different solid samples, was turned into an advantage for permittivity measurements of a fixed duct where a fluid flows, thanks to the process of calibrating device (see § "Procedure").

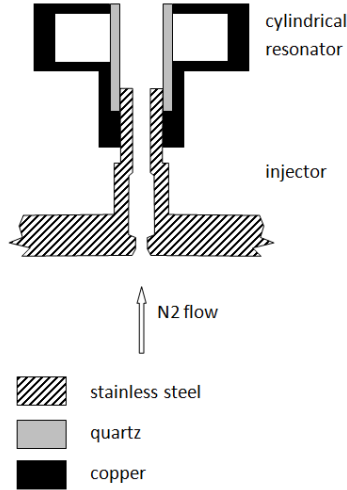


Fig. 5. Resonance cavity at injector exit

Using the Lorentz-Lorenz formula [30-31] developed for homogeneous isotropic media or statistically homogeneous and isotropic two-phase media and recently reconsidered by [32], we used an expression of the relative dielectric permittivity of the media proportional to the density through the number density of molecules in the medium N (see also [33]):

$$\frac{\varepsilon(\omega)-1}{\varepsilon(\omega)+2} = \frac{4\pi N}{3} \overline{\alpha}_e(\omega) \quad (16)$$

The mean polarizability $\overline{\alpha}_e(\omega)$ at frequency ω is not a linear function of the resonance frequency ω_0 and therefore the permittivity is not a linear function of the resonance frequency ω_0 . However, on a short range of values it was shown that it could be considered as a linear relation without inducing significant error. Leblond & Stepowski [26] recommended a range of frequencies less than several hundreds of MHz (our experiment range was 100MHz) and permittivity $1 < \varepsilon < 2$ (N2 flow gives the bounds $\varepsilon_{LN2} = 1.43$ and ε_{GN2} very close to 1 [34]). Our simulations confirmed the negligible error (less than 1/10000) as obtained elsewhere [23]. This allowed us to formulate the two following equations fundamental to link the measured resonance frequency and the two-phase flow density. Considering two media with known dielectric permittivity ε_1 and ε_2 associated to the respective resonance frequency ω_1 and ω_2 when put one after another in place of the studied two-phase flow inside the resonator, the linearity finding gives:

$$\frac{\varepsilon_m - \varepsilon_1}{\varepsilon_2 - \varepsilon_1} = \frac{\omega_m - \omega_1}{\omega_2 - \omega_1} \quad (17)$$

and equation (16) is rewritten:

$$\frac{\varepsilon_i - 1}{\varepsilon_i + 2} = K \omega_i \quad (18)$$

where K is a constant which can be determined experimentally during the calibrating process and the subscript refers to the medium considered.

Introducing:

$$\delta\omega = \omega_m - \omega_1 \quad (19)$$

$$\Delta\omega = \omega_2 - \omega_1 \quad (20)$$

$$\Delta\varepsilon = \varepsilon_2 - \varepsilon_1 \quad (21)$$

equation (17) becomes :

$$\varepsilon_m = \frac{\delta\omega}{\Delta\omega} \Delta\varepsilon + \varepsilon_1 \quad (22)$$

which gives into (18) for the two-phase flow density ($i=m$) :

$$\rho_m = \frac{1}{K} \frac{\frac{\delta\omega}{\Delta\omega} \Delta\varepsilon + \varepsilon_1 - 1}{\frac{\delta\omega}{\Delta\omega} \Delta\varepsilon + \varepsilon_1 + 2} \quad (23)$$

Equation (23) was used to calculate ρ_m from ω_m . Uncertainty calculation and application with values of the experiments led to estimate uncertainty on ρ_m less than 2.5%.

Another source of uncertainty was due to the fact that equation (16) was developed for statistically homogeneous isotropic media such as spherical inclusions inside a continuous milieu. If the size of inclusions does not matter provided that their size remains smaller than the wavelength of the probing wave, their shape or their arrangement are important factors of possible uncertainty [26]. We carried out test experiments in order to evaluate the influence of these parameters. Using periodical solid structures of polycarbonate and polyethylene and controlled two-phase flow of air/cyclohexane (having permittivity differences close to that of LN2-GN2), the density measured by the resonator differed less than 3% from the expected values.

The last possible contribution to the density uncertainty was link with the temperature resonator stability as pointed out elsewhere [35-36]. The tests undertaken with the mock-up showed a maximum deviation of .3MHz for the resonance frequency (coherent with results of [36]) leading to less than .3% of uncertainty for density.

As argued above in this section, the cavity was designed for TM₀₁₀ resonance mode considering three coaxial media bounded by a , b , c , respectively internal and external radius of the duct made of quartz (Pyrex, $\varepsilon=3.8$) and internal radius of the cavity made of copper. Using Maxwell equations, the TM₀₁₀ mode was described by a system of five equations where the components of the electromagnetic field were expressed in terms of Bessel functions of first and second kinds. Its resolution allowed us to adjust a resonance frequency equals to 8GHz with radius in mm (a , b , c) = (1.5, 2.5, 12.5) and an internal length of the cavity equal to 6.4mm.

The cavity was coupled by a metal ring inserted into the cavity and connected to a sweep generator according to the description made by Leblond & Stepowski [26]. It enabled to provide an incident microwave signal with linear frequency and to detect the reflected signal which was absorbed by the cavity at the resonance value, giving therefore the value of the resonance frequency varying with the two-phase flow density. The incident signal swept a range of 100MHz around 8GHz over 5ms (in coherence with the response time of the pressure lines).

2.2.4 Resulting uncertainty on the mass flow

Taking into account all these considerations exposed in section 2.2 and the contribution of

the slip factor correlation using Premoli et al.'s [19] (§2.1), uncertainty calculation from equation (7) led to estimate the uncertainty on G equal to 7.2%.

2.3. Procedure

Two experimental conditions were studied:

- Condition 1 with inert gas sweep before opening the LN2 valve only,
- Condition 2 with inert gas sweep before opening the LN2 valve and 150ms after.

In both conditions, the time $t=0$ was associated with the opening of the LN2 valve which was closed 300ms after. Data acquisition was performed during these 300ms.

2.3.1 Calibration phase

The constant K of equation (18) had to be experimentally determined. For this aim, the N2 two-phase flow was replaced by liquid cyclohexane at ambient temperature: $\epsilon=2.02$ at 20°C [37:p508]. From this value and the associated resonance frequency, the value of K was determined and then used for calculation of the density of the two-phase flow.

2.3.2 Pre-injection phase

Pre-injection phase preceded the opening of the LN2 valve. Inert gas He (mass flow .1g/s) was injected inside the duct in order to eject any solid particle or droplet of water that could stay inside. During this time, the volume reproducing the LOXdome was lowered in temperature by means of an external flow of LN2. This phase lasted 3 minutes.

2.3.3 Injection phase

The LN2 valve was opened at $t=0$. According to the experimental condition, He sweep was stopped at $t=0$ (condition 1) or at $t=150$ ms (condition 2). The data acquisition was stopped at $t=300$ ms and LN2 valve was closed.

3. RESULTS

Conditions 1 and 2 both exhibited unstable flows illustrated by oscillatory characters of the acquired data.

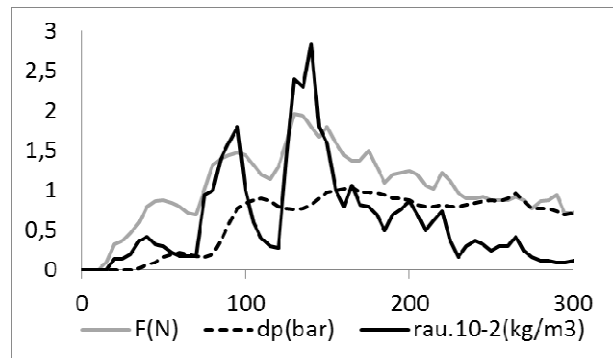
In both conditions, a high rate of reproducibility was observed for each test of each given condition: amplitude and wavelength of the measurement curves (F , dp and ρ_m) were similar from one to another.

3.1. Condition 1

Condition 1 was N2 flow with He sweep flow stopped at $t=0$.

Figure 6 presents variations of the physical quantities needed in equation (7) to calculate the mass flow G which is drawn on Figure 7. Impact force, pressure drop as well as density oscillate around an increasing slope during the first 140ms and then around a decreasing slope (less pronounced for dp) as part of an oscillation of longer wavelength. Additional experiments lasting several seconds have shown that this was the case, showing a 15Hz oscillation superimposed to a 1.5 to 3Hz wave during several seconds. Data Figure 6 show G oscillates before $t=160$ ms with large amplitude and then decreases to about 5g/s. Mean and max values are given in Table 1.

324



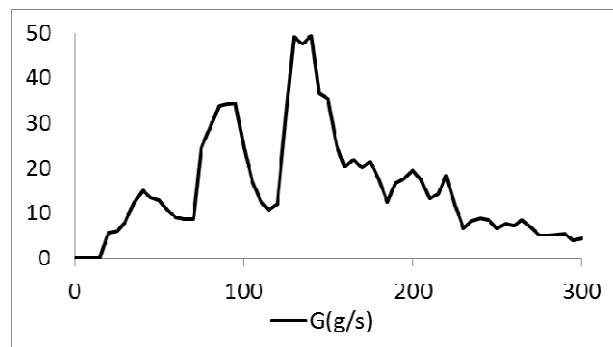
325

326

327

Fig. 6. Impact force F (N), pressure drop dp (bar) and fluid density ρ_m (kg/m³) during 300ms after opening the LN2 valve (condition 1).

328



329

330

331

Fig. 7. N2 mass flow G (g/s) calculated during 300ms after opening the LN2 valve (condition 1).

332

333

334

Table 1. Mean and maximum values for physical quantities of eq. (7) – condition 1

Quantity	F (N)	dp (bar)	ρ_m (kg/m ³)	G (g/s)
Mean	1.03	.63	63.24	15.69
Max	1.96	1.04	284.00	49.49

335

336

337

338

339

340

Figure 8A & B presents mass flow G vs pressure drop dp during 300ms. From zero, the points describe two loops from $t=0$ to 150ms oscillating for the last loop on a large range of G but a narrow range a dp , then decrease to 5g/s while dp stabilizes between 0.8 and 1bar.

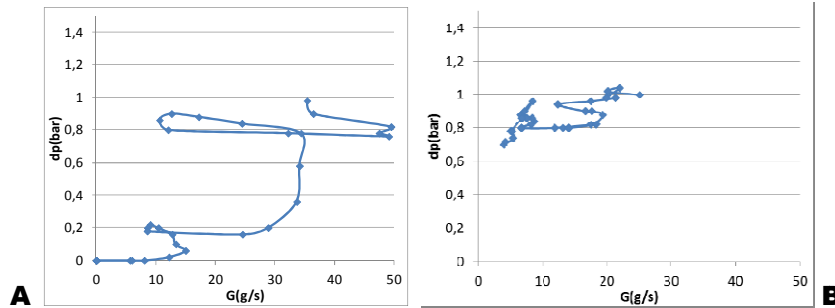


Fig. 8. N2 mass flow G (g/s) vs pressure drop dp A) during the first 150ms after opening the LN2 valve and B) during the following 150ms (condition 1).

3.2. Condition 2

Condition 2 was N2 flow with He sweep flow stopped at $t=150$ ms.

Figure 9 presents variations of the physical quantities needed in equation (7) to calculate the mass flow G which is drawn on Figure 10. Impact force and density oscillate around an increasing slope during the first 100ms, then around a decreasing slope and stabilize after $t=160$ ms, making G oscillating before $t=160$ ms and then stabilizing around 10g/s. Pressure drop increases during the first 150ms and then decreases. Mean and max values are given in Table 2.

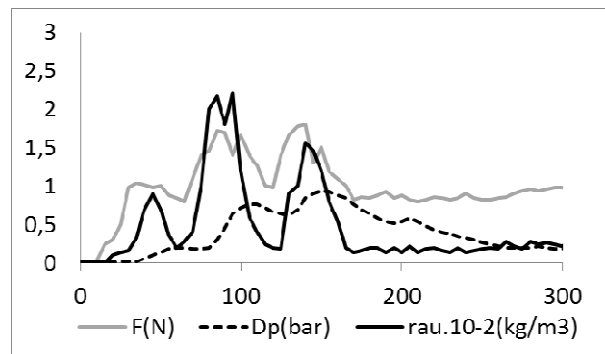


Fig. 9. Impact force F (N), pressure drop dp (bar) and fluid density ρ_m (kg/m³) during 300ms after opening the LN2 valve (condition 2).

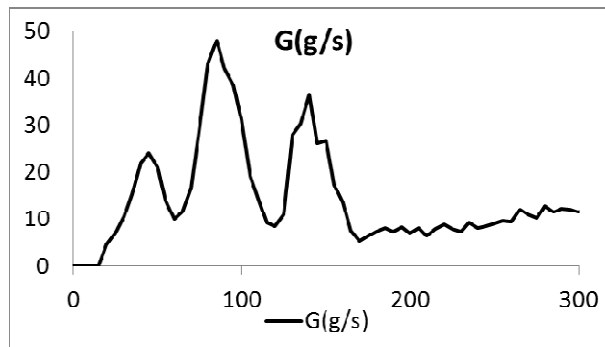


Fig. 10. N2 mass flow G (g/s) calculated during 300ms after opening the LN2 valve

361 (condition 2).

362

363 **Table 2. Mean and maximum values for physical quantities of eq. (7) – condition 2**

364

Quantity	F (N)	dp (bar)	ρ_m (kg/m ³)	G (g/s)
Mean	.98	.39	47.73	14.41
Max	1.80	.94	222.00	47.98

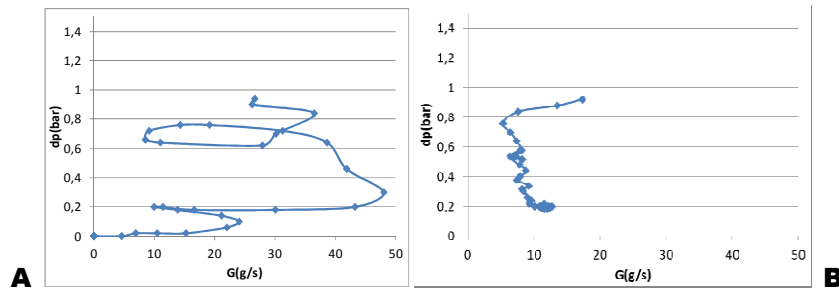
365

366 Figure 11A & B presents mass flow G vs pressure drop dp during 300ms. From zero, the

367 points describe two loops from $t=0$ to 150ms oscillating for the last loop on a large range of

368 G but a narrow range a dp , then decrease to and stabilize about 10g/s while dp to .2bar.

369



370

371 **Fig. 11. N2 mass flow G (g/s) vs pressure drop dp A) during the first 150ms after**
372 **opening the LN2 valve and B) during the following 150ms (condition 2).**

373 4. DISCUSSION

374

375 4.1. General considerations

376

377 Discussion of the results may take benefits of previous studies undertaken by Hu et al. [38]
378 who analyzed N2 vertical flows inside a 8mm diameter pipe and complemented their
379 measurements by video analysis through high speed camera recordings. In similar
380 conditions to the present experiments, Hu et al. clearly identified a chilldown process when
381 N2 entered the pipe involving dramatic flow pattern development: Hu et al.'s results suggest
382 that at the earliest stage and at high mass flow rate (according to Hu et al.'s criteria,
383 conditions 1 and 2 are high mass flow rates), the flow is characterized by inverted annular
384 flow and then mist flow, a dispersed flow comprised of small and spherical liquid drops
385 embedded in the gas. They also explain that this occurs while the wall temperature is higher
386 than the rewetting temperature.

387

388 Fu et al. [39] undertook similar investigations for vertical N2 flow in 1.931mm internal
389 diameter duct, focusing on stabilized flows. They elaborated several types of two-phase flow
390 regime maps devoted to N2 among which one in terms of mass flux vs quality. Comparing
391 our data to their results, it appears clearly that the flows studied in the present research were
392 of annular type, in accordance with the above description based on Hu et al.'s results.

393

394 Furthermore, findings and conclusions of Qi et al. [40] who also undertook studies of LN2 in
395 microtubes (diameter 0.931mm) led to consider these types of annular or mist flows as
396 homogeneous. Qi et al. explained that, in micro-tube at high mass flux, homogeneous flow

was favored by the small density ratio of liquid to vapor and the small viscosity of liquid nitrogen favoring mixing of liquid and vapor phases. Despite the fact that their work concerned long lasting flows displaying lower frequencies, the classification they proposed for stable/unstable N2 flow in 1.931mm diameter duct located conditions 1 and 2 of the present study in unstable region which is coherent with the curves obtained.

It is tempting to relate oscillations observed in conditions 1 and 2 to the pressure drop oscillation (PDO) phenomenon due to the existence of the LOXdome just upstream the injector as well as to density wave oscillation (DWO) mechanism due to vaporization of LN2 in the injector, the former sustaining the latter. However these kinds of instabilities are associated with large amplitude excursion of the physical quantities and low frequency oscillations [15], conversely to what was obtained here. High frequency oscillations are usually related to acoustic oscillations linked with resonance of pressure waves inside the considered system and related to the time needed for the pressure waves to propagate in the system. The frequency identified in §3.1 (1.5 to 3Hz and 15Hz) are typical of thermo-acoustic oscillations (TAO) [41-43]. The following analysis will help us to suggest hypothesis for the mechanism encountered in the experiments.

4.2. Comparative analysis

When the mass flow curves for conditions 1 and 2 are superimposed (Figure 12), similar oscillations are observed especially in terms of extrema localization of the first three oscillations but their amplitudes differ.

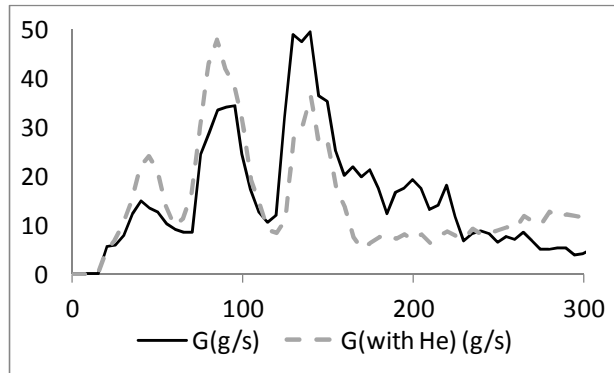


Fig. 12. Time comparison of N2 mass flow calculated from $t=0$ to $t=300$ ms for condition 1 (G) and for condition 2 (G with He)

This difference of amplitude leads to a better mass flow in condition 2. Comparison of values in Tables 1 and 2 suggests the opposite mean and max values are higher for condition 1, but when comparing time variation, it is clear that during the first 120ms and from $t=270$ ms to the end, condition 2 gave higher mass flow than condition 1 (Figures 12 & 13); from 120 to 270, it was opposite; this gave an equal time of higher mass flow for each condition. In addition, during the last 150ms, mass flow was stable in condition 2 (Figures 10, 11B, 12, 14) around 10g/s whereas condition 1 gave a decreasing and unstable mass flow (Figures 7, 8B, 12, 14). The final mass flow in condition 2 was twice this of condition 1.

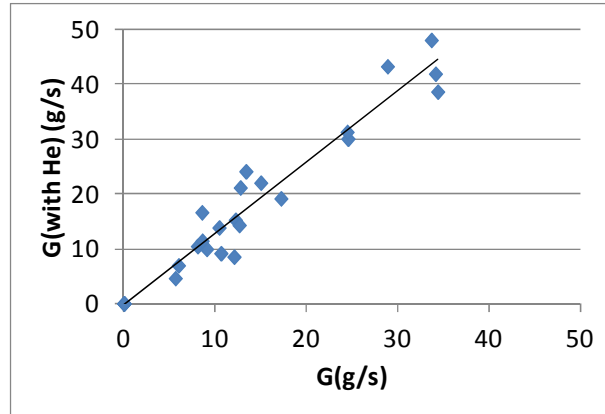


Fig. 13. Relative comparison of N2 mass flow calculated from t=0 to t=120ms for condition 1 (G) and for condition 2 (G with He); $r=0.96$

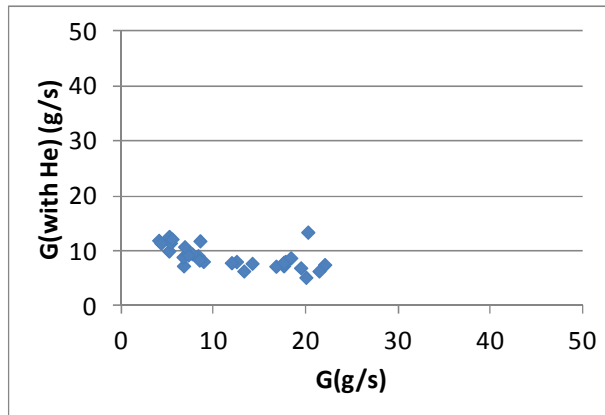


Fig. 14. Relative comparison of N2 mass flow calculated from t=160 to t=300ms for condition 1 (G) and for condition 2 (G with He)

These results indicate that He sweeping mass flow had a stabilizing effect. This could be due to the fact that He flow contributed to reduce the heat flux from the injector wall over time by reducing the difference of temperature with the fluid and at the same time led to a vaporization of the LN2 in the volume of fluid (condition 2) rather than from the wall (condition 1) contributing therefore to homogenizing the two-phase flow. In addition, the vaporization process was more efficient in condition 2 (as attested by density measurements shown Figures 6 and 9) and contributed to make the flow speed closer to the sound speed in the fluid and therefore to the critical flow conditions. Applying Hosangadi et al.'s correlation developed for sound speed in two-phase flows whilst studying cavitation on cryogenic fluids [44]:

$$v_{sound,m} = \frac{1}{\sqrt{\rho_m}} \left\{ \frac{\alpha}{\rho_g v_{sound,g}^2} + \frac{1-\alpha}{\rho_l v_{sound,l}^2} \right\}^{-1/2} \quad (24)$$

we found that condition 2 was a critical flow all along the 300ms and for condition 1 the flow was critical except over two time slots of 10ms each corresponding to the higher values of ρ_m . yet the Mach number was higher in condition 2 than 1. This critical flow was induced especially by the internal geometry of the injector with the restricted nozzle at inlet.

Despite the fact that TAO have been investigated for space rocket engines, these concerned

instabilities generated in the combustion chamber after ignition during nominal operations (see the review [45]). Conversely, out the combustion domain, the literature is poor. In their recent review, Ruspini et al. [42] reported that "It is worth noting that in some cases TAO are observed together with other phenomena (in particular with geysering and DWO); this is especially the case for transient flows. Nevertheless, the interaction between these high frequency phenomena and the other oscillatory phenomena is not investigated". They noticed however that oscillatory behavior found during heat transfer to a fluid occurred regardless of whether the fluid was at a subcritical or supercritical pressure.

These considerations suggest that the main difference between conditions 1 and 2 lies in the heat transfer change due to the relative high temperature gas in the mixture during the prolonged sweep of He in condition 2. Indeed, He gas sweep increased the interface between N2 and a medium with higher temperature than N2: N2-wall interface in condition 1; N2-wall interface and N2-He interface in condition 2. Such increase of interface reduces the temperature difference between the wall and the mixture. All other parameters being identical from one condition to another and oscillations amplitude being higher in condition 1 than in condition 2 (see tables 1 and 2), we may assume that the thermal effect was major in favoring thermo-acoustic oscillations (which is different from triggering) in condition 1 compared to condition 2. The stability map of Ishii and Ishii & Zuber [46] based on the dimensionless subcooling and phase change numbers may help us to understand the stabilizing effect of He: the stabilizing effect of He might be explained by the reduction of the heat flux (the phase change number is lessened) combined with the reduction of the inlet subcooling enthalpy (the subcooling number lessened) thus moving the operating point on the map towards a more stable zone.

Applying these findings to the LOX flow of the rocket engine, it suggests the promotion of prolonged He sweep.

Some worries could rise regarding an associated lower feeding rate of O2 for the combustion chamber due to presence of He and thus resulting in a lower mixture ratio. Hence having a more stable mass flow by means of prolonged He sweep might be seen as a drawback by lowering the mixture ratio but we argued at the beginning of this section that mass flow in condition could not be strictly considered lower than in condition 1; furthermore, even if so, Mastorakos et al. [47] showed that favorable ignition conditions required poor stoichiometric mixture: the shortest starting time for engine ignition was obtained for poor mixtures i.e. far away from stoichiometric conditions.

5. CONCLUSION

Studying the pre-ignition transient in one full scale injector of HMB7 engine (equipping Ariane 5 launcher) with N2 flow in thermo-hydrodynamic conditions of similitude with O2, we found that a prolonged sweep of the injector with inert gas (He) had a stabilizing effect on the flow during the transient phase before ignition of the engine. This finding is of great importance for space rocket engineering as stabilizing the flow may contribute to guaranty the expected early ignition of cryogenic engines.

Analysis led to characterize the flow as inverted annular flow and then mist flow (dispersed flow comprised of small and spherical liquid drops embedded in the gas). The homogeneous character of the flow was favored by the small density ratio of liquid to vapor and the small viscosity of liquid nitrogen inducing mixing of liquid and vapor phases. The flow was found critical with instabilities analyzed as being thermoacoustic oscillations (TAO). Thermal effect was identified as major in the production of these oscillations. Characterization of the

stabilizing effect of He prolonged sweep was explained through reduction of wall heat flux and of the inlet subcooling enthalpy. This finding is of great interest as it shows that TAO are generated in the unit engine much earlier than after ignition inside the combustion chamber and may help researchers to adapt or reconsider the existing combustion models: even if the oscillation mechanisms are likely quite different in terms of source of instabilities and of factors sustaining instabilities, we might assume a coupling effect between both during ignition and make the hypothesis of a non-negligible effect of the former on the latter at least during ignition.

Further experiments are required to better characterize and control the stabilization effect of prolonged inert gas sweep as TAO phenomenon is of importance for engines: high frequency pressure oscillations may destroy and ruin not only injectors but the ignition unit as a whole.

Further experiments are also required to quantify the stabilizing effect in terms of heat flux and of subcooling enthalpy: a better understanding may be of great benefits for the future re-ignited engines developed today for future space flights as each (re)ignition phase is a stage with non-negligible probability of failure.

Symbols & Units

Symbol	Quantity	Units
α	void fraction	none
$\overline{\alpha}_e(\omega)$	mean polarizability at frequency ω	$\text{C}^2.\text{m}^2.\text{J}^{-1}$
β	coefficient	none
$\delta\Delta$	difference	none
η	dynamic viscosity	$\text{kg}/(\text{m}.\text{s})^{-1}$
ε	relative dielectric permittivity	F/m
γ	surface tension	N/m
ρ	Density	kg/m^3
ω	frequency	Hz
ω_0	resonance frequency	Hz
A	area	m^2
a, b, c	radius	m
d	diameter	M
dp		
$E_{1,2}$	coefficients	none
f, F	force	N
G	mass flow	kg/s

N	Number density of molecules	unit
p	pressure drop	Pa
Re	Reynolds number	none
r	Correlation coefficient	none
s	slip ratio	none
T	temperature	K
t	time	S
v	velocity	m/s
We	Weber number	none
X	vapor quality	none
y	coefficient	none

Subscripts

Symbol	Relates to:
i	generic subscript taking other values
l	liquid
g	gas
$exit$	injector exit
m	mixture; two-phase fluid
$sound$	sound

Abbreviations

Symbol	Definition
He	helium
LOX	Liquid oxygen
LN2/GN2	Liquid / Gas nitrogen
N2	nitrogen
O2	oxygen

COMPETING INTERESTS

The author has declared that no competing interests exist.

REFERENCES

1. Ravet L. The ARIANE 5 launcher improvements. Air & Space Europe. 2000;2(2): 68-72.

- 546 2. Sippel M, Klevanski J, Burkhardt H, Eggers T, Bozic O, Langholf P, Rittweger A.
547 Progress in the Design of a Reusable Launch Vehicle Stage. AIAA. 2000: Paper 5220.
- 548 3. Sippel M, Herbertz A, Haeseler D, Götz A. Feasibility of High Thrust Bleed Cycle
549 Engines for Reusable Booster Applications. 4th International Conference on Launcher
550 Technology-Space Launcher Liquid Propulsion. 2002:3-6.
- 551 4. Kitsche WH. Re-ignitable gas generator cycle rocket engine. 4e Eor. Conf. for
552 Aerospace Sc. (EUCASS, St-Petersburg, Russia). 2011.
- 553 5. Dumont E, Burkhardt H, Sippel M, Johannsson M, Ludwig, C, David E. Exploiting
554 technological synergies for future launch vehicles. 4th International Conference-Space
555 Technologies: Present and Future. 2013.
- 556 6. Haydn OJ. Advanced rocket engines. Advances on Propulsion Technology for High-
557 Speed Aircraft. 2008;(1):6.1-6.40.
- 558 7. Cho N, Kim S, Kim Y, Jeong S, Jung J. Two-phase flow characteristics of liquid oxygen
559 flow in low pressure liquid rocket engine. Cryogenics. 2004;44(6):493-500.
- 560 8. Caisso P, Souchier A, Rothmund C, Allio P, Bonhomme C, Zinner W, Parsleyd R, Neille
561 T, Fordee S, Starkee R, Wang W , Takahashi M, Atsumi M, Valentian, D. A liquid
562 propulsion panorama. Acta Astronautica, 2009;65(11):1723-1737.
- 563 9. Alliot P, Dalbies E, Delie V, Ruault JM. Overview of the development progress of the
564 VINCI engine- 2003. 54 th International Astronautical Congress of the International
565 Astronautical Federation(IAF). 2003.
- 566 10. Micaelli JC, Spindler B, Momponteil A. Thermohydraulique diphasique pour Ariane: un
567 exemple de diffusion technologique. La Houille Blanche. 1995(1):54-57.
- 568 11. Spies J. RLV Hopper: Consolidated system concept. Acta Astronautica. 2003;53(4):
569 709-717.
- 570 12. Gröning S, Suslov D, Oschwald M, Sattelmayer T. Stability behaviour of a cylindrical
571 rocket engine combustion chamber operated with liquid hydrogen and liquid oxygen. 5th
572 European Conference for Aeronautics and Space Sciences, EUCASS, Munich,
573 Germany. 2013.
- 574 13. Popp M, Stanke J. Experimental investigation of the HM7B thrust chamber start-up
575 transient. 24th Joint Propulsion Conference. 1988:paper 2931.
- 576 14. Kitsche W. Operation of a Cryogenic Rocket Engine. Berlin: Springer. 2011.
- 577 15. Kakac S, Bon B. A review of two-phase flow dynamic instabilities in tube boiling
578 systems. International Journal of Heat and Mass Transfer. 2008;51(3):399-433.
- 579 16. Di Matteo F, De Rosa M, Onofri M. Start-up transient simulation of a liquid rocket
580 engine. Joint Propulsion Conferences, American Institute of Aeronautics and
581 Astronautics. 2011 :Paper 6032.
- 582 17. McManus TN. Management of Hazardous Energy: Deactivation, De-energization,
583 Isolation, and Lockout. CRC Press. 2012.
- 584 18. Isselhorst A. HM7B Simulation with ESPSS Tool on Ariane 5 ESC-A Upper Stage. 46th
585 AIAA/ASME/SAE/ASEE Joint Propulsion Conference & Exhibit. 2010; paper 7047.
- 586 19. Premoli A., Francesco D, Prima A. An empirical correlation for evaluating two-phase
587 mixture density under adiabatic conditions. European Two-Phase Flow Group Meeting,
588 Milan, Italy. 1970.
- 589 20. Yashar DA. Experimental investigation of void fraction during horizontal flow in smaller
590 diameter refrigeration applications. Air Conditioning and Refrigeration Center. College of
591 Engineering. University of Illinois at Urbana-Champaign. 1998.

- 592 21. Woldesemayat MA, Ghajar AJ. (). Comparison of void fraction correlations for different
593 flow patterns in horizontal and upward inclined pipes. *International Journal of*
594 *Multiphase Flow*. 2007;33(4):347-370.
- 595 22. Krupka J. Frequency domain complex permittivity measurements at microwave
596 frequencies. *Measurement Science and Technology*. 2006;17(6):R55.
- 597 23. Paez EJ, Callarotti RC, Sanchez Y. Measurable Dielectric Permittivity Range for TE and
598 TM Modes in a Shielded Dielectric Resonator. *Journal of Electromagnetic Analysis and*
599 *Applications*. 2015;7(06):189-197.
- 600 24. Prakash V, Roberts JA. Perturbation of a resonant microwave cavity by select alcohol
601 vapors. *J. Microwave Power*. 1986;23:45-50.
- 602 25. Fauquet Ph. Dispositif hyperfréquence pour mesure de densité en écoulement
603 diphasique transitoire [Hyperfrequency device for measurement of transient two-phase
604 flow density]. Doctoral dissertation. Paris: Un. P. & M. Curie. 1991. French.
- 605 26. Leblond J, Stepowski D. Some non-intrusive methods for diagnosis in two-phase flows.
606 *Multiphase Science and Technology*. 1994;8(1-4):715-782.
- 607 27. Filippov YP. How to measure void fraction of two-phase cryogenic flows. *Cryogenics*.
608 2001;41(5):327-334.
- 609 28. Filippov YP, Kakorin ID, Kovrizhnykh AM. New solutions to produce a cryogenic void
610 fraction sensor of round cross-section and its applications. *Cryogenics*. 2013;57:55-62.
- 611 29. Kinzer JP, Wilson IG. Some results on cylindrical cavity resonators. *Bell System*
612 *Technical Journal*. 1947;26(3):410-445.
- 613 30. Lorentz HA. Über die Beziehung zwischen der Fortpflanzungsgeschwindigkeit des
614 Lichtes der Körperdichte [On the relationship between of the speed of light of the milieu
615 density] *Ann. Phys.* 1880;9:641-665. German.
- 616 31. Lorenz L. Über die Refractions constante [About refraction constant] *Ann. Phys.*
617 1880;11:70-103. German.
- 618 32. Oughstun K, Cartwright N. On the Lorentz-Lorenz formula and the Lorentz model of
619 dielectric dispersion. *Optics express*. 2003;11(13):1541-1546.
- 620 33. Ryzhov YA, Tamoikin VV, Tatarskii VI. Spatial dispersion of inhomogeneous media.
621 *Soviet Phys. JETP*. 1965 ;21(2):433-438.
- 622 34. Suda Y, Itoh M, Sakai Y, Matsuura K, Honma N, Kimura T. Behaviour of liquid nitrogen
623 between electrodes in a microgravity environment. *Cryogenics*. 1996 ;36(8):567-571.
- 624 35. Jacob MV, Mazierska J, Ledenyov D, Krupka J. Microwave characterisation of CaF₂ at
625 cryogenic temperatures using a dielectric resonator technique. *Journal of the European*
626 *Ceramic Society*. 2003;23(14):2617-2622.
- 627 36. Ishizaki T. Temperature-stable dielectric TM₀₁₀-mode resonator and its application to
628 compact base station filter. *IEICE Electronics Express*. 2010;7(6):454-459.
- 629 37. Zhou Y. *Physicochemical Measurements: Catalogue of Reference Materials from*
630 *National Laboratories*. Elsevier. 2013.
- 631 38. Hu H, Chung JN, Amber SH. An experimental study on flow patterns and heat transfer
632 characteristics during cryogenic chilldown in a vertical pipe. *Cryogenics*.
633 2012;52(4):268-277.
- 634 39. Fu X, Qi SL, Zhang P, Wang RZ. Visualization of flow boiling of liquid nitrogen in a
635 vertical mini-tube. *International journal of multiphase flow*. 2008;34(4):333-351.
- 636 40. Qi SL, Zhang P, Wang RZ, Xu LX. Flow boiling of liquid nitrogen in micro-tubes: Part I—
637 The onset of nucleate boiling, two-phase flow instability and two-phase flow pressure

- 638 drop. International journal of heat and mass transfer. 2007;50(25):4999-5016.
- 639 41. Smirnov HF, Zrodnikov VV, Boshkova IL. Thermoacoustic phenomena at boiling
640 subcooled liquid in channels. International journal of heat and mass transfer.
641 1997;40(8):1977-1983.
- 642 42. Ruspini LC, Marcel CP, Clausse A. Two-phase flow instabilities: A review. International
643 Journal of Heat and Mass Transfer. 2014 ;71:521-548.
- 644 43. Tadrist L. Review on two-phase flow instabilities in narrow spaces. International Journal
645 of Heat and Fluid Flow. 2007;28(1):54-62.
- 646 44. Hosangadi A, Ahuja V, Ungewitter RJ. Simulations of cavitating cryogenic inducers.
647 AIAA. 2004:paper 4023.
- 648 45. O'Connor J, Acharya V, Lieuwen T. Transverse combustion instabilities: Acoustic, fluid
649 mechanic, and flame processes. Progress in Energy and Combustion Science.
650 2015;49:1-39.
- 651 46. Ishii M, Zuber N. Thermally induced flow instabilities in twophase mixtures. Proc. Fourth
652 Int. Heat Transfer Conf. on Heat Transfer. 1970;(5):paper B5.11.
- 653 47. Mastorakos E, Baritaud TA, Poinso TJ. Numerical simulations of autoignition in
654 turbulent mixing flows. Combustion and Flame. 1997;109(1):198-223.